Korean J. Chem. Eng., 32(9), 1853-1863 (2015)
DOI: 10.1007/s11814-015-0017-y

pISSN: 0256-1115
eISSN: 1975-7220

Improving water permeability and anti-fouling property of polyacrylonitrile-based hollow fiber ultrafiltration membranes by surface modification with polyacrylonitrile-*g*-poly(vinyl alcohol) graft copolymer

Noor Aina Mohd Nazri, Woei Jye Lau, and Ahmad Fauzi Ismail†

Advanced Membrane Technology Research Centre (AMTEC), Universiti Teknologi Malaysia, 81310 Skudai, Johor, Malaysia
(*Received 17 June 2014 • accepted 23 January 2015*)

Abstract–The effect of polyacrylonitrile-*g*-poly (vinyl alcohol) (PAN-*g*-PVA) copolymer additive on the properties of PAN-based hollow fiber UF membranes was studied. The resulting hollow fiber membranes were characterized with respect to structural morphology, surface properties, and proteins rejection in order to investigate the impact of PAN-*g*-PVA copolymer composition (presented at different PAN : PAN-*g*-PVA ratio) in the UF membrane on the separation and antifouling properties. Results showed that the hollow fiber membrane prepared from the highest composition of PAN-*g*-PVA copolymer (PAN : PAN-g-PVA 80 : 20) was able to produce pure water flux as high as 297 L/m^2·hr in comparison to 41 L/m^2·hr reported in control PAN membrane when tested at 1 bar. Fouling experiments performed using bovine serum albumin (BSA), albumin from chicken egg (CE) and trypsin indicated that the blend membranes with higher surface coverage of hydrophilic PVA (34-60%) were more excellent in minimizing protein fouling, which might be correlated with the formation of hydrophilic PVA layer on their surface. Although increase in membrane hydrophilicity upon PAN-*g*-PVA copolymer incorporation might be the main reason contributing to improved membrane antifouling properties, the changes in membrane surface roughness and pore size could not be completely ruled out to influence membrane anti-fouling resistance during protein filtration.

Keywords: Amphiphilic Copolymer, Ultrafiltration, Polyacrylonitrile, Anti-fouling, Poly(vinyl alcohol), Protein

INTRODUCTION

Ultrafiltration (UF) membranes have been widely employed in wide ranges of industrial applications such as food and manufacturing, biomedical, wastewater treatment, and water purification due to their exceptional advantages such as low operating cost, high permeability and ambient temperature operation [1,2]. However, a common problem encountered in UF membrane process is the fouling problem, which represents a challenge to the widespread implementation of this process in various applications [3]. The undesirable fouling phenomenon is typically associated with nonspecific deposition and/or adsorption of proteins or other biomolecules from the feed water onto membrane surface and/or pore walls, causing severe flux decline and a decrease in membrane efficiency [4-6].

Various approaches have been proposed in an attempt to enhance fouling resistant by improving membrane hydrophilicity to inhibit hydrophobic interaction between the foulants and the membrane matrix [3,7]. In general, the modification approaches can be classified into surface coating [8,9], surface grafting [10], plasma treatment [11,12], and blending process [13,14]. Of these methods, the blending method remains the most popular modification technique in the preparation of UF membrane due to its simplicity and effectiveness in producing desired membrane properties. Currently, direct blending membrane with amphiphilic copolymer has drawn great attention from scientists owing to the unique self-organizing behavior of the copolymer during phase inversion process. Theoretically, the self-organizing behavior involves migration of hydrophilic chain towards aqueous environment and anchoring of hydrophobic chain on hydrophobic membrane matrix [15], which could offer better stability, higher degree of compatibility and also efficient separation and anti-fouling performance [6]. For example, Liu et al. [16] reported an increase in both permeability (up to 510 L/m^2·hr·bar) and anti-fouling performance when poly (vinylidene fluoride)-*g*-poly(ethylene glycol) methyl ether methacrylate (PVDF-*g*-PEGMA) was used as additive in making PVDF-based membrane. Shi et al. [17], on the other hand, incorporated polysulfone-*g*-poly(N-methyl-D-glucamine) (PSF-*g*-PNMG) to PSF-based membrane in which they found that the modified PSF membrane exhibited higher permeation flux of 470 L/m^2·hr·bar with flux recovery recorded at 95% after a simple cleaning process, in comparison to 125 L/m^2·hr·bar and 80% reported in unmodified PSF membrane. The promising results are attributed to the increase in membrane surface hydrophilicity as well as formation of open porous structures.

Although a number of studies report the viability of using UF membrane made of only PAN polymer for aqueous solution separation processes, the critical issue - fouling problem is the main challenge of the sustainable operation of PAN-based membrane in long run [18,19]. Therefore, incorporating PAN-based membrane with amphiphilic copolymer additive is helpful to improve membrane anti-fouling performance and prevent flux decline [15]. As shown in Table 1, only several reports are found available in open

†To whom correspondence should be addressed.
E-mail: afauzi@utm.my

Table 1. The use of amphiphilic copolymers in fabrication of PAN-based membranes

Membrane	Method of copolymer synthesis	Optimized dope formulation	Optimized membrane properties	Remarks
[a]Main polymer: PEG-*g*-PAN [5]	Water phase precipitation	PEG molecular weight was varied: 400, 1,000, 2,000, 4,000, 6,000 Da Polymer composition: 15 wt% Solvent: DMF	MW of PEG: 2,000 Da Contact angle: 38.8° [c]PWF: 294.4 L/m^2·hr·bar Protein adsorption: 5.8 μg/cm^2 Protein rejection ratio: 93.5% Flux recovery: 91.6%	Selecting appropriate molecular weight is crucial in controlling membrane properties and performance.
[a]Main polymer: PAN Copolymer additive: PAN-*g*-PEO [15]	Free polymerization	PEGA added during reaction (wt%): 15-50 PAN-*g*-PEO composition: 0-20 wt% Solvent: DMF	PEGA added during copolymer synthesis: 50 wt% Wetting time: 8.4 s [c]PWF: 159.0 L/m^2·hr·bar Flux recovery: 100% BSA retention: 89% Sodium alginate retention: 12% Humic acid retention: 84%	Higher PEO content in copolymer of up to 60% could lead to membrane water solubility.
[a]Main polymer: PAN Copolymer additive: PAN-*r*-DMMSA [20]	Water phase suspension polymerization	DMMSA content varied from 0-5.8 mol% Mass of PAN: 0-3.9 g Mass of PAN-*r*-DMMSA: 0-3.9 g Mass of DMSO: 26.1 g DMMSA mol fraction: 0-5.8 mol PAN-*r*-DMMSA mass fraction: 0-100	DMMSA content: 5.8 mol% Contact angle: 42.5° PWF: 276.61 L/m^2·hr·bar Protein retention: 70% Flux recovery: 95%	Higher DMMSA content tends to reduce porosity and increase membrane thickness, hence resulting flux reduction.
[a]Main polymer: PAN-*b*-PEG [21]	Combined redox polymerization and reversible addition fragmentation	PEG content in copolymer was varied ranging from 0-11.1 mol%. MW of PEG: 5,000, 10,200, 23,500 Da Polymer composition: 10 wt% Solvent: NMP	PEG composition in copolymer: 11.1 mol% Contact angle: 45° [c]PWF: 218.9 L/m^2·hr·bar BSA rejection: above 98.4% Protein adsorption: 24.3 μg/cm^2 Increased resistance: 9%	Copolymer composition plays a significant role in controlling membrane structure, properties and performance, while effect of PEG molecular weight in copolymer commonly negligible.

[a]Flat sheet
[b]Molecular weight
[c]Pure water flux

literature for PAN membrane modification using amphiphilic polymers [5,15,20,21]. In view of this, in the present work, an amphiphilic graft copolymer bearing hydrophilic PVA and PAN segments was first synthesized via $Ce^{(IV)}$-initiated free radical polymerization, followed by incorporation of it in the PAN dope solution for membrane surface modification. PVA was adopted as the hydrophilic segment to prepare the amphiphilic graft copolymer due to its outstanding properties such as highly hydrophilic, good membrane forming property, biocompatibility as well as good physical and chemical stability [7]. The utilization of PVA in amphiphilic copolymer preparation has great potential to modify membranes to be effective not only in resisting fouling but also improving water permeability. Yet, despite the beneficial features of PVA, very few studies reported on the modification of UF membranes with PVA. This is probably due to the complicated and difficult copolymer preparation procedures [22].

While flat sheet PAN-based membranes have been frequently studied, PAN membranes in hollow fiber configuration have been less researched. In our recent work, the effect of the amount of acrylonitrile (AN) monomer added during PAN-*g*-PVA amphiphilic copolymer synthesis and its relationship to the properties and performance of PAN-based hollow fiber membranes was systemati-

cally investigated. It was found that the membrane properties (i.e., morphology, surface roughness, surface chemical composition and hydrophilicity) and performance (i.e., pure water permeation and anti-fouling) were obviously altered upon the addition of the copolymer with different properties (mol% of PVA in copolymer and number of PVA repeating units) [23]. As a continuation of the previous work, special focus is given in this study to investigate the effect of the graft copolymer composition in the dope solution and its correlation to membrane properties and performance. The changes in membrane surface characteristics were evaluated using X-ray photoelectron spectroscopy (XPS), atomic force microscopy (AFM) and scanning electron microscopy (SEM) and contact angle goniometer. Anti-fouling performances of the resulting membranes were assessed via filtration experiments with the use of feed solution containing different types of foulants: bovine serum albumin (66 kDa), albumin from chicken egg (45 kDa) and trypsin (20 kDa).

EXPERIMENTAL

1. Materials and Reagents

PAN-based UF hollow fiber membranes were prepared using polyacrylonitrile (PAN, M_W: 150,000 g/mol) purchased from Sigma Aldrich. Poly(vinyl alcohol) (PVA, M_W: 61,000 g/mol) with degree of polymerization 1400 was purchased from Fluka. Dimethyl sulfoxide (DMSO, ACS grade, assay 99.9%) and ceric ammonium nitrate (CAN, 0.1 M) purchased from Sigma Aldrich were used as a solvent and initiator of graft copolymer synthesis, respectively, without further purification. Analytical reagent grade monomer, acrylonitrile (AN, M_W: 53.06 g/mol) was supplied by Merck. Albumin from bovine serum (BSA), albumin from chicken egg (CE) white and trypsin were all purchased from Sigma Aldrich.

2. Synthesis of PAN-g-PVA

The typical synthesis route of PAN-*g*-PVA amphiphilic copolymer was as follows. The $Ce^{(IV)}$-initiated free radical polymerization was carried out in a round bottom flask equipped with a mechanical stirrer. The nitrogen gas was bubbled through the system to maintain inert condition inside the system. 10 g PVA was firstly dissolved in DMSO at 60 °C. After the solution was cooled to room temperature, 10 g AN monomer and 10 mL Ceric (IV) stock solution were added to the solution while maintaining the reaction temperature at 50-60 °C. The system was sealed and the reaction was allowed to proceed for 4 hr. The mixture was then precipitated in excess acetone, filtered by vacuum suction and dried in vacuum oven overnight. Proposed reaction mechanism of the PAN-*g*-PVA copolymer is shown in Fig. 1. The characteristics of synthesized PAN-*g*-PVA copolymer were analyzed by Fourier transform infrared (FTIR) spectroscope (Perkin-Elmer Spectrum One) and ^{1}H NMR spectroscope (Bruker Avance 400) to ascertain chemical bonding and structure of the copolymer. The resulting graft copolymer details are presented in Table 2.

3. Membrane Preparation

The PAN/PAN-*g*-PVA blend membranes were prepared via phase inversion process. To prepare a dope solution, desired amounts of PAN and the synthesized copolymer that was weighted previously were added into DMSO solvent to achieve desired weight ratio of PAN/copolymer in dope solution. The total concentration of PAN and the copolymer was kept at 12 wt% in the solution; the composition of each doped solution is shown in Table 3. The mixture was continuously stirred using IKA RW20 digital mechanical stirrer at 60 °C until permanent homogeneous solution was formed. The homogeneous dope solution was then degassed prior to spinning process.

The hollow fiber membranes were fabricated via dry-jet wet spinning process. The dope solution was extruded through a spinneret with 0.55 mm inner diameter and outside diameter of 1.10 mm while the injection rate of internal coagulant was kept constant at 2.0 mL/min. Then, the as-spun hollow fibers were passed through

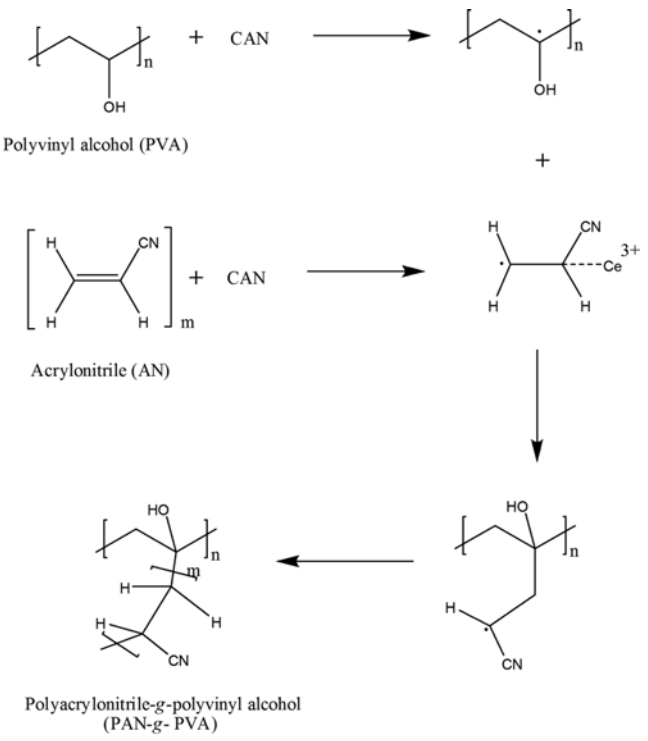

Fig. 1. Proposed reaction mechanism of the synthesized graft copolymer.

Table 2. Details of PAN-*g*-PVA graft copolymer

AN : PVA ratio	1 : 1
% Grafting (%G)[a]	127.9
% Grafting efficiency (%GE)[a]	127.9
Mol% of PVA in graft copolymer[b]	92.6

[a]Computed from gravimetric analysis
[b]Calculated from ^{1}H NMR

Table 3. Spinning dope composition

Sample code	PAN : PAN-*g*-PVA mass ratio[a]
PAN	100 : 0
CP10-5	95 : 5
CP10-10	90 : 10
CP10-20	80 : 20

[a]Total polymer concentration in dope solution is 12 wt%

Table 4. Spinning conditions of PAN-based UF hollow fiber membrane

Dope extrusion rate (mL/min)	4-5
Bore fluid	Pure water
Bore fluid flow rate (mL/min)	2.0
External coagulant	Pure water
Air gap distance (cm)	5
Spinneret O.D/I.D (mm/mm)	1.10/0.55
Coagulation temperature (°C)	25

5 cm air gap before being guided through two water coagulation baths at take-up velocity of 10.32 cm/s. It is assumed that the take-up velocity was nearly the same with the free falling velocity of the hollow fibers. The nascent hollow fibers were then post-treated with 10 vol% glycerol in water for three days before drying. After drying, the hollow fibers were ready for testing. The detailed spinning conditions are listed in Table 4.

4. Membrane Characterization

The surface and cross-section morphologies of the hollow fiber membranes were observed using a scanning electron microscope (SEM) (TM3000, Hitachi). The membranes were immersed and fractured in liquid nitrogen and then were sputtered with gold before analysis. The SEM images of cross sectional area and surface were taken at different magnifications.

Surface chemical composition of the hollow fiber membranes was evaluated by X-ray photoelectron spectroscope (XPS) (Kratos Axis HS X-ray photoelectron spectrometer, Kratos Analytical). This analysis was performed using Al K_α X-radiation as the X-ray source. The take-off angle was set at 90°. The full range survey spectra of the hollow fiber UF membranes were collected over a range of 0-1,200 eV.

Degree of hydrophilicity of UF membranes was evaluated by tangent method using contact angle system (OCA 15pro, DataPhysics Instruments). The hollow fibers were cut and deionized water of 0.3 μL was dispersed from microsyringe onto the membrane surface. An average value of 15 different measurements was taken to report.

Surface topography and roughness of the membranes were investigated by atomic force microscope (AFM) using tapping mode nanoscope III equipped with a 1553D scanner (SPA-300 HV, Seiko). A small piece of hollow fiber membrane was cut and glued on 1 cm^2 square paper card. The root mean square (RMS) was used to determine the surface roughness of the hollow fiber membrane based on 3.0 μm×3.0 μm scan area. The images were captured and were presented in 3D diagram.

5. Ultrafiltration Experiment

Lab-scale cross flow filtration system was setup and used to investigate the separation performance of the prepared hollow fiber membranes. Membrane module was designed to have approximately 72.25 cm^2 effective surface area (10 fibers in 20 cm long) and was tested in outside-in filtration mode. Feed solution was transferred from solution tank to membrane housing using a low pressure booster pump. Prior to flux determination, the hollow fiber membranes were firstly compacted at 1.5 bar for at least 30 min to achieve steady flux. All the UF experiments were performed at ambient temperature and pressure of 1 bar. Initial pure water flux (J_{W1}) was then calculated by using Eq. (1).

$$J_{W1}=\frac{v}{t\times A} \quad (1)$$

where v is the volume of permeated water (L), t is permeation time (hr) and A is the effective membrane area (m^2). For protein rejection analysis, the solution tank was filled up with 1.0 g/L protein solution and the protein flux (J_p) was recorded in accordance to Eq. (1). Protein rejection (R) was then determined using Eq. (2).

$$R=\left(1-\frac{C_p}{C_f}\right)\times 100\% \quad (2)$$

where C_p and C_f are the protein concentrations (mg/mL) of permeate and feed solutions, measured by UV-vis spectrophotometer (DR5000, Hach), respectively. After the filtration of protein solution, the membranes were cleaned thoroughly by filtering DI water for 30 min. Then, the pure water flux (J_{w2}) of membrane was measured again. To determine anti-fouling performance of the hollow fiber membranes, flux recovery (*RFR*) reversible (*Rr*) and irreversible (*Rir*) fouling were determined as follows:

$$RFR(\%)=\left(\frac{J_{W2}}{J_{W1}}\right)\times 100 \quad (3)$$

$$Rr(\%)=\frac{J_{W2}-J_P}{J_{W1}}\times 100 \quad (4)$$

$$Rir(\%)=\frac{J_{W1}-J_{W2}}{J_{W1}}\times 100 \quad (5)$$

RESULTS AND DISCUSSION

1. Characterization of PAN-*g*-PVA Copolymer

The chemical structure of the synthesized copolymer was ascertained by FTIR and further confirmed by ^1H NMR. Fig. 2 shows the IR spectra of the PAN-*g*-PVA copolymer. The appearance of the peak at 2,400 cm^{-1} signifies the presence of CN group while the broad and strong band at 3,424 cm^{-1} is assigned to hydroxyl group

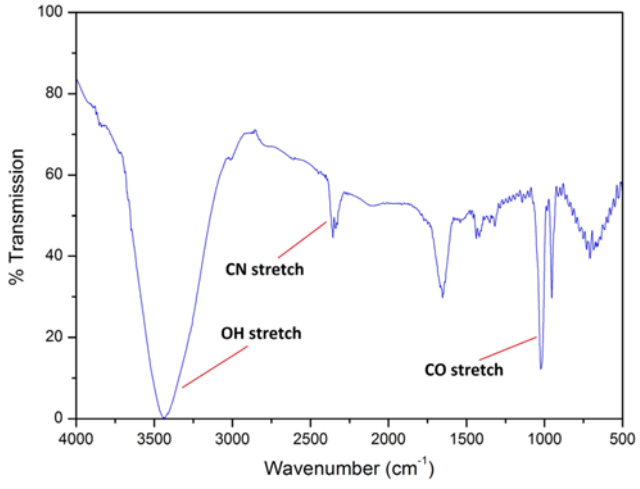

Fig. 2. FTIR spectrum of the PAN-*g*-PVA copolymer.

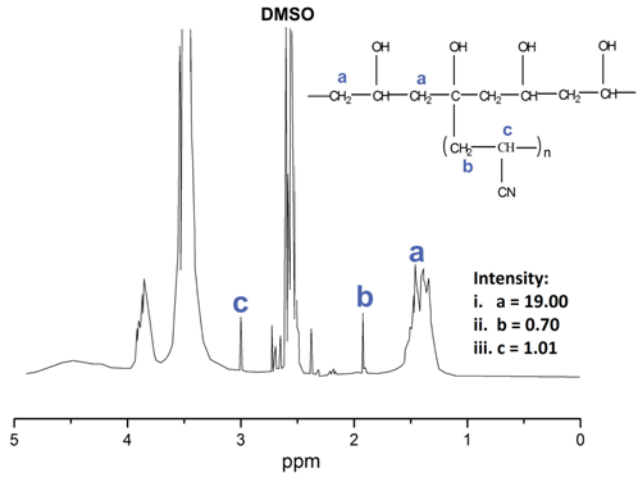

Fig. 3. ^{1}H NMR spectrum of the PAN-*g*-PVA copolymer.

(OH). Additionally, the sharp peak recorded at around 1,017 cm^{-1} is attributed to the C-O stretching vibration of PVA. On the other hand, the NMR peaks with the chemical shift and proposed chemical structure of the PAN-*g*-PVA copolymer are presented in Fig. 3. The resonance of the two protons of the CH_2-CH-CN is found at δ=1.9-20 ppm. Meanwhile, the resonance at δ=3.0 ppm could be assigned to a proton bonded to C-CN and the two protons connected to C-OH showed chemical shift at δ=1.4-1.6 ppm. The presence of vital peaks and resonances in the IR and ^{1}H NMR spectra confirmed the formation of PAN-*g*-PVA copolymer.

2. Compatibility between PAN-*g*-PVA Graft Copolymer and PAN Polymer

One of the simplest methods of predicting the thermodynamic compatibility of two polymer blends is by determining solubility parameter difference. Table 5 presents the solubility parameters which are determined according to group contribution method [24]. As a rule, for compatible polymer blend, the difference in solubility parameter δ_T between the two blend polymers must be less than 0.5 [25]. As can be seen from the table, the difference in solubility parameter ($\Delta\delta_T$) of PAN and that of graft copolymer is obtained as follows: CP10-5=0.08, CP10-10=0.15, and CP10-20=0.3. The low values of $\Delta\delta_T$ imply that blending PAN with PAN-*g*-PVA graft copolymer is theoretically compatible and that the value of solubility parameter difference only increases slightly with increasing graft copolymer composition in the PAN dope solution.

3. The Morphological Properties of the PAN/PAN-*g*-PVA Membranes

As depicted in Fig. 4, membrane cross-sectional morphology was observed by SEM at 400× magnification. The cross-section of the prepared membranes shows typical asymmetric structure for UF membrane. It can be clearly seen that the cross-section of the prepared membranes composes finger-like macrovoids extending across both outer and inner walls of the hollow fiber with either sponge-like structure (in control membrane) or macroporous substructure (in blend membranes) as intermediate layer. Generally, the morphology of cross-section is mainly influenced by the polymer solution behavior during phase inversion process [26]. It can be observed that the length of the finger-like structure near the outer wall is longer than those on the lumen side. This might be associated with the immediate demixing process soon after the membrane extruded from the tip of the spinneret and passed through a short air gap of 5 cm. It is seen that the incorporation of PAN-*g*-PVA copolymer affects the membranes selective skin layer. The skin layer thickness of the blend membranes is significantly thinner than the control PAN membrane and this is likely due to the relatively faster demixing process promoted by the hydrophilic PVA in blend membranes. The SEM micrographs also revealed no significant morphological differences between the membranes incorporated with low content of PAN-*g*-PVA copolymer, i.e., CP10-5 and CP10-10. However, the microporous substructure enlarged with the increase of PAN-*g*-PVA copolymer content in dope solu tion: CP10-20. Furthermore, the finger-like macrovoids at the intermediate layer are found to merge and connect with the macrovoids near the lumen, forming an irregular size of macrovoids.

Fig. 5 shows the SEM surface images (10,000× magnification) of the membranes prepared from the blending of PAN and PAN-*g*-PVA copolymer. Additional insight into the morphological properties of the hollow fiber membranes with respect to surface porosity and pore size was obtained using ImageJ software [27]. The surface pore size (dp_{avg}) and porosity (ε) of the membranes together with their contact angle and pure water flux (PWF) are presented in Table 6. It can be evidently observed that both pore size and poros-

Table 5. Hansen solubility parameters

Membrane code	[a]δ_d (MPa)$^{1/2}$	[b]δ_p (MPa)$^{1/2}$	[c]δ_h (MPa)$^{1/2}$	[d]δ_t (MPa)$^{1/2}$	[e]$\Delta\delta_t$ (MPa)$^{1/2}$
PAN	15.7	14.0	23.6	31.6	–
PVA	16.2	22.8	7.2	28.9	–
DMSO	18.4	16.4	10.2	26.7	–
CP10-5	15.7	14.1	23.7	31.7	0.08
CP10-10	15.8	14.2	23.7	31.8	0.15
CP10-20	15.9	14.3	23.7	31.9	0.30

[a]δ_d=Dispersive interaction
[b]δ_p=Dipolar interaction
[c]δ_h=Hydrogen bond
[d]δ_t=Solubility parameter
[e]$\Delta\delta_t$=Solubility parameter difference

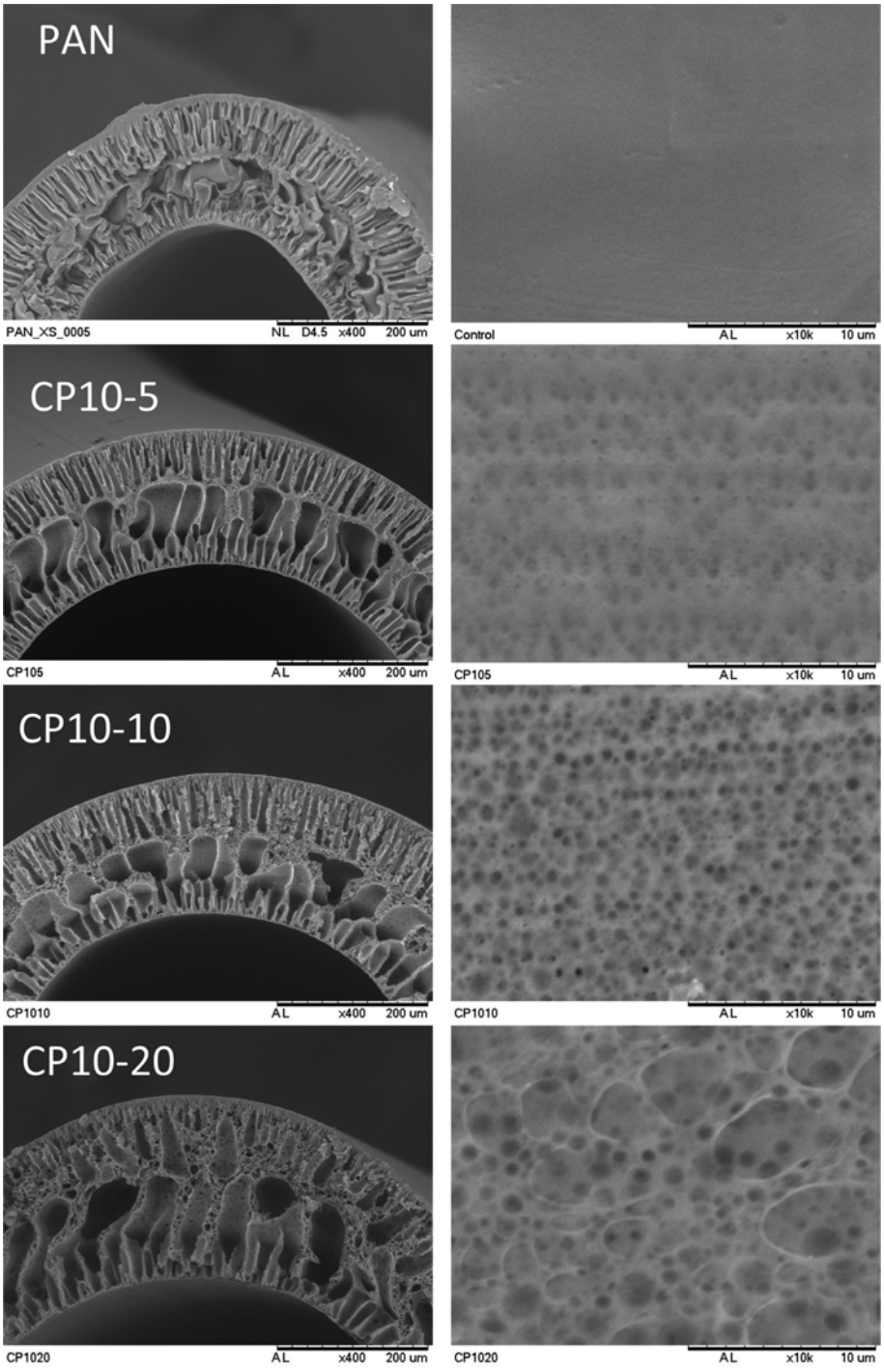

Fig. 4. Cross-sectional and surface morphologies of PAN control membrane and the blend membranes.

ity increase with increasing PAN-*g*-PVA copolymer content in the PAN-based membrane. This might be attributed to the instantaneous demixing process induced by the presence of the graft copolymer in the dope system. The measured surface pore size increases according to CP10-5 (15 nm)<CP10-10 (36 nm)<CP10-20 (45 nm). With respect to membrane porosity, the membrane tends to become more porous with increasing the graft copolymer composition in the PAN dope solution. The results obtained are consistent with the previous work in which amphiphilic copolymer is used as additive in UF membrane preparation [17]. It must be mentioned that the porosity of the PAN control membrane is not able to detect from its SEM surface image, mainly due to its small pore size. On the other hand, CP10-5 and CP10-10 blend membranes are found to have a uniform pore size, which might be attributed to the highly compatible blend solution.

Previous works have reported the role of amphiphilic copolymer in changing the morphological properties of UF membranes [21,26]. In this work, we also found that the incorporation of PAN-

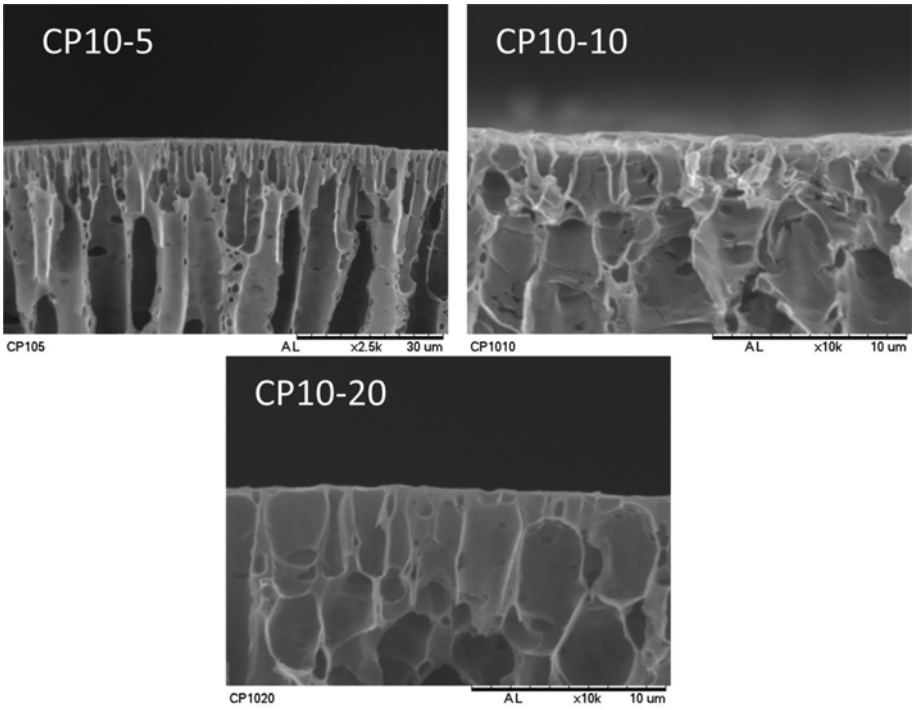

Fig. 5. Cross-sectional SEM images of the top layer of the blend membranes at 10k magnification.

Table 6. Properties of fabricated PAN-based hollow fiber membranes

Membrane	Contact angle (°)	dp_{avg} (nm)[a]	ε (%)[b]	J_{W1} (L/m^2·hr)[c]
PAN	75.99±1.76	3	9	41±1.94
CP10-5	53.13±2.30	15	21	137±0.55
CP10-10	62.73±1.48	36	23	140±1.70
CP10-20	63.23±1.91	45	27	297±6.66

[a]Average pore size
[b]Porosity
[c]Pure water flux

g-PVA copolymer additive is beneficial in improving morphological properties of the PAN-based UF membranes. As shown in Fig. 5, with increasing PAN-*g*-PVA copolymer content in the dope solution, the morphological structure near the outer of membrane tends to alter from long finger-like structure, as evidenced in CP10-5 membrane to bigger finger-like macrovoids in CP10-20 membrane. The significant change in morphological structure is likely to increase membrane water permeation rate, owing to reduced transport resistance.

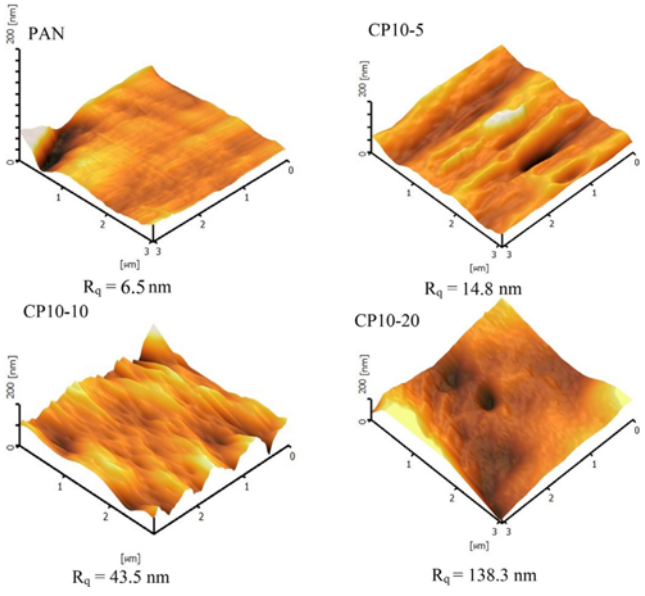

Fig. 6. AFM topography images of the hollow fiber membranes.

4. The Surface Properties of the Hollow Fiber Membranes

Fig. 6 presents the 3D AFM images of the PAN membranes blended with and without PAN-*g*-PVA copolymer. From these images, the surface roughness of PAN-based UF membrane is significantly altered upon addition of PAN-*g*-PVA copolymer in which the higher the content of copolymer added in dope solution, the greater the membrane surface roughness produced. The measured RMS value for the control PAN membrane is only around 6.5 nm in comparison to 14.8, 43.5 and 138.3 nm reported for CP10-5, CP10-10 and CP10-20 membrane, respectively. The main factor contributing to the significant increase in surface roughness is the fast demixing process promoted by the presence of hydrophilic PVA component in the dope solution. To confirm the existence of PVA in the membrane matrix, an XPS analysis near the top surface of the membranes was conducted and the results are shown in Table 7.

Theoretically, during phase inversion process, PAN-*g*-PVA copolymers would reorganize themselves in order to reduce interfacial energy of membrane and create a stable state of minimum free energy. Consequently, the self-organization behavior of the copoly-

Table 7. A summary of atomic percentage on membrane surface and degree of PVA surface coverage on the hollow fiber membranes

Membrane	Atomic percentage from XPS (at%)			C[a] (%)
	C	O	N	
PAN	75.55	7.92	16.53	23.78
CP10-5	71.58	19.95	8.46	59.91
CP10-10	75.98	11.39	12.64	34.20
CP10-20	74.73	10.49	14.78	31.50

[a]The degree of PVA surface coverage

mer would result in simultaneous migration of hydrophilic PVA towards aqueous water environment [28]. In this regard, XPS analysis could provide beneficial data on the successful migration of PVA to the membrane surface. To quantitatively illustrate the coverage of hydrophilic PVA on membrane surface, the degree of PVA surface coverage, C was computed using the following equation [5].

$$C(\%) = \frac{T_o}{M_o} \times 100 \quad (6)$$

where T_o is the oxygen molar ratio on membrane surface which was determined from XPS analysis. M_o is the theoretical oxygen molar ratio if the membrane surface is completely covered with PVA chain. Table 7 summarizes the atomic percentage and degree of PVA surface coverage on the hollow fiber membranes. A low concentration of oxygen (O) (7.92%) was detected on the surface of PAN control membrane, which might be due to residual solvent or adsorbed oxygen from air. It can also be seen that O concentration (indicate the presence of -OH functional group) and degree of PVA surface coverage increase while nitrogen (N) concentration (indicate the presence of -CN functional group) decreases in the blend membranes compared to the control membrane. These results imply the migration of PVA towards the membrane surface. The theoretical O/N (based on dope composition) and obtained O/N values from the XPS analysis are also determined and results are shown in Fig. 7. All the blend membranes exhibit higher O/N mole ratio compared to the control membrane and remarkably show higher value of O/N than those of the corresponding theoretical values, which further confirms the favorable enrichment of PVA segment on membrane surface rather than to disperse uniformly in the membrane bulk.

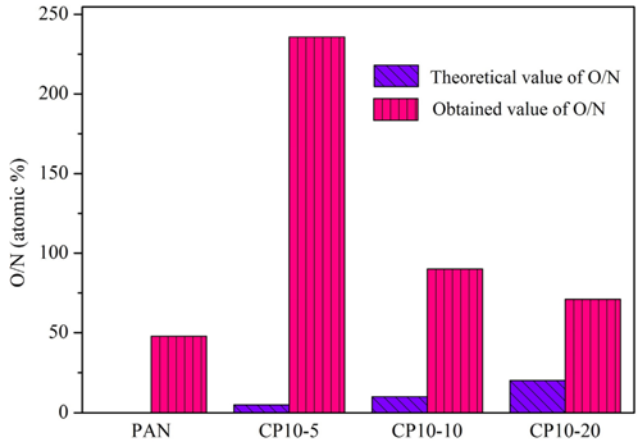

Fig. 7. O/N values on the surface of the hollow fiber membranes.

Theoretically, CP10-20 membrane should have the highest PVA concentration on the membrane surface due to presence of high composition of PAN-*g*-PVA in the membrane matrix. However, the surface composition of the prepared membranes shows the opposite trend in which CP10-5 membrane displays the highest concentration of PVA, while CP10-20 membrane the lowest: CP10-5 (59.91%)>CP10-10 (34.20%)>CP10-20 (31.50%). On the other hand, the average content of PVA component in the membrane is CP10-20 (18.52%)>CP10-10 (9.26%)>CP10-5 (4.63%). It can be inferred from these results that the surface segregation of graft copolymer has occurred. Thus, the lowest surface coverage of PVA in CP10-20 membrane is probably because the increase in the copolymer composition in dope solution reduces the mobility and flexibility of PVA hydrophilic segments (due to increase in dope viscosity), which tends to slower the migration of PVA towards the membrane surface. Furthermore, the significant increase in surface roughness promoted by the increase of copolymer composition may also affect the XPS results. Additionally, the addition of graft copolymer additive can enhance the rate of demixing process, causing the phase inversion to occur very fast in the dope solution containing high composition of graft copolymer. The subsequent short time might inhibit the migration of PVA segments to the membrane surface. Note that during phase inversion, the solidification step and surface segregation of copolymer occur simultaneously [16,29].

It is predicted that any change in surface chemical composition is accompanied by change of surface hydrophilicity. Thus, contact angle analysis is carried out to evaluate the hydrophilicity of the membrane surface and the results are presented in Table 6 together with pore size and porosity of the membranes and the membranes performance during filtration process. It can be observed from the table that the contact angle is firstly reduced from 76° in the control PAN membrane to 53.1° for CP10-5 membrane upon addition of copolymer additive. Further increase in copolymer content causes the membrane contact angle to increase as shown in CP10-10 (62.7°) and CP10-20 membrane (63.2°). The change in contact angle is consistent with the variation of surface elemental composition shown in Table 7, which suggests the effect of surface composition on membrane hydrophilicity.

5. Filtration Performance

It can be clearly seen from Table 6 that the pure water flux of membrane is improved with increasing copolymer composition in

Table 8. Rejections of proteins by the hollow fiber membranes

Membrane code	*R* (%)		
	BSA	CE	Trypsin
[a]PAN	100	-	-
CP10-5	100	98.24	74.26
CP10-10	99.91	96.88	71.45
CP10-20	99.47	95.50	64.79

[a]The rejection of the PAN membrane is only evaluated using BSA

the PAN dope solution in which the CP10-20 membrane achieves the highest flux, recording close to 297 L/m^2·hr in comparison to only 41 L/m^2·hr achieved by the control PAN membrane. The significant improvement of the pure water flux is mainly due to the increase in membrane surface pore size and/or overall porosity, and partially contributed by the improved surface hydrophilicity and surface roughness as well (increase in the efficient area for filtration).

Besides membrane water flux, the effect of graft copolymer composition in dope solution on protein rejection is also studied and

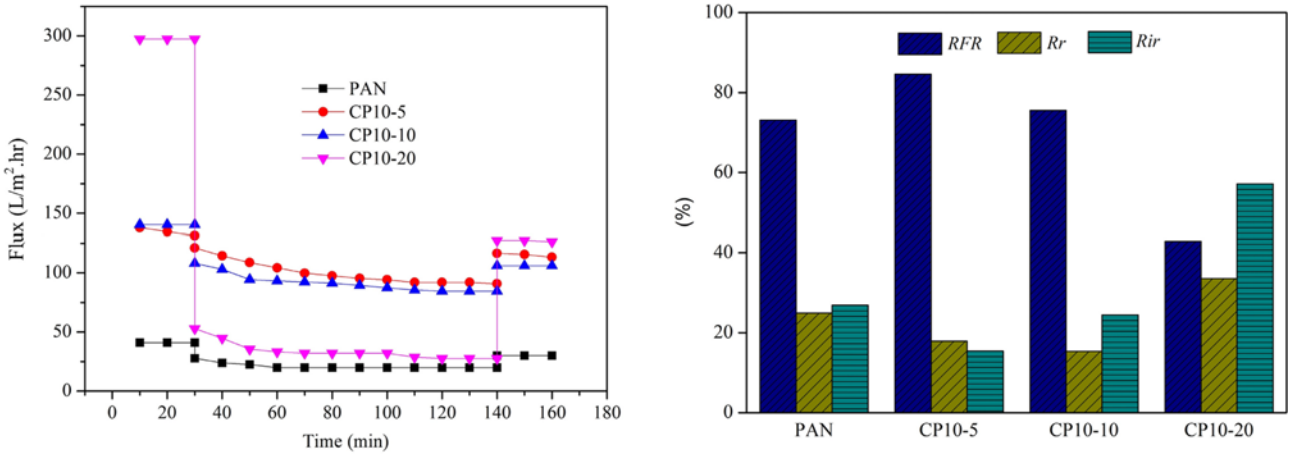

Fig. 8. Time-dependent fluxes of the hollow fiber membranes and a summary of the corresponding *RFR*, *Rr* and *Rir* during BSA solution.

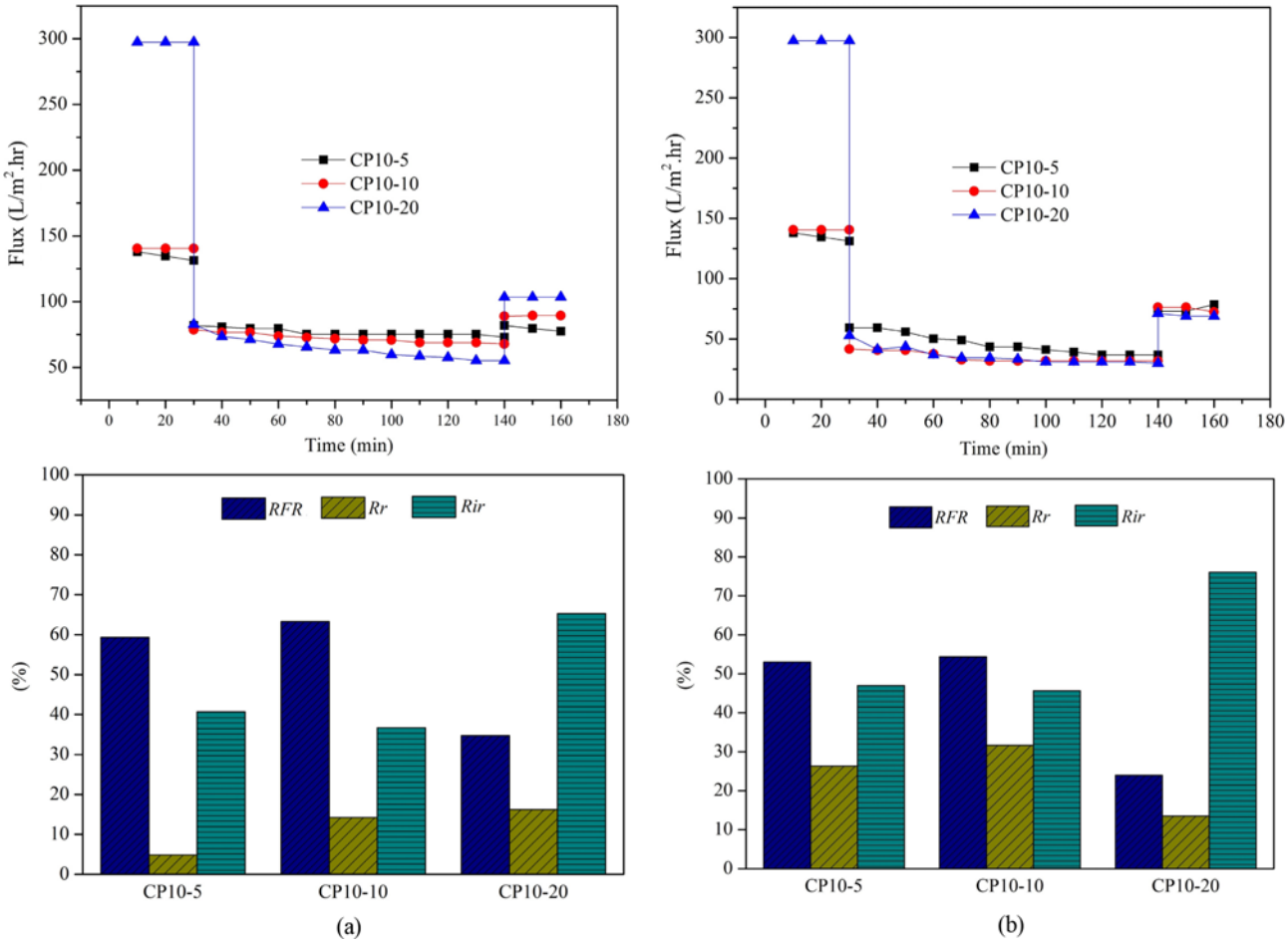

Fig. 9. Time-dependent fluxes of the hollow fiber membranes and a summary of the corresponding *RFR*, *Rr*, and *Rir* during (a) CE solution, and (b) trypsin solution.

the results are shown in Table 8. It is reported that almost complete BSA rejection is able to be achieved regardless of the membrane properties, indicating the pore size of membranes prepared is much smaller than the size of the BSA. However, decreasing the MW of the test proteins (CE and trypsin) decreases the separation efficiency of the blend membranes gradually. When comparing rejection performance of the blend membranes, CP10-5 membrane shows significantly better proteins rejection due to its smaller surface pore size than the other blend membranes.

6. Membrane Anti-fouling Performance

Fig. 8 shows the time dependent fluxes for the prepared membranes during 2-hr filtration of BSA solution**.** Additional insight into the anti-fouling behavior of the membranes with respect to flux recovery (*RFR*), reversible fouling (*Rr*) and irreversible fouling (*Rir*) are also investigated, and the results are tabulated in Fig. 9. The control PAN membrane shows initial flux of around 41 L/m^2·hr; this value however decreases by 51.8% during BSA filtration, mainly owing to the formation of cake layer resulted from deposition and adsorption of BSA protein on membrane surface. A simple cleaning process is found to be able to retrieve close to 75% of the membrane water flux, revealing the flux decline is mainly governed by reversible fouling. We also do not rule out the relatively smooth surface (RMS: 6.5 nm) of the control membrane itself partly reducing the fouling extent. Even though the control PAN membrane exhibits good fouling resistance to a certain extent, the relatively low water permeability makes it impractical for industrial adoptions. Of the blend membranes tested, the CP10-5 membrane displays the highest flux recovery, 84.6% in comparison to 75.5% and 42.9% found in CP10-10 and CP10-20 membranes, respectively. In addition, the lowest *Rr* and *Rir* values demonstrated by CP10-5 membrane could be well-correlated to its low surface roughness (14.83 nm), good hydrophilicity (53.13°) and highest coverage of hydrophilic PVA (59.91%). The highest flux recovery obtained in CP10-5 membrane is also probably due to its smaller pore size, by which the large BSA molecules could not enter the small pore size, minimizing pore blockage phenomenon due to adsorption of BSA in the inner pores. As previously reported, factors such as membrane hydrophilicity, surface roughness and surface chemical composition are also the key parameters governing the severity of fouling [21,30,31]. Note the excellent fouling resistance of CP10-5 membrane is consistent with the high surface coverage of PVA shown by the membrane, which prevents protein adsorption and enhances fouling resistant. These results are in agreement with the previous studies that indicated the importance of surface chemical composition on membrane anti-fouling property [5,15,25].

The anti-fouling property of the blend membranes was further investigated using CE and trypsin as model foulants and the time-dependent fluxes for the blend membranes are presented in Fig. 9. The flux recovery behavior of the membranes CP10-5 and CP10-10 during CE and trypsin filtrations is significantly greater than CP10-20 membrane, indicating the presence of sufficient amount of PVA on membrane surface could induce greater fouling resistant. Comparing the results of BSA filtration with trypsin and CE filtration, the flux recovery of the blend membranes tends to decrease when smaller foulants are used. The decreasing size of foulants might have caused not only protein deposition on membrane surface but also adsorption within membrane internal pores, leading to pore narrowing/blockage and further increasing the degree of irreversible fouling as evidenced in this work.

As seen in Fig. 9, the trend of anti-fouling property of the blend membranes during filtration of CE and trypsin is slightly different from the BSA filtration. For instance, highest *RFR* of 63% (CE filtration) and 54% (trypsin filtration) are achieved by the CP10-10 membrane which possesses lower degree of PVA surface coverage (34.2%) and higher contact angle (62.7°). On the other hand, CP10-5 membrane with 59.9% degree PVA surface coverage and 53.3° reveals rather lower *RFR* of 59% (CE filtration) and 53% (trypsin filtration). This phenomenon may be explained by the enhancement of pore constricting and/or pore blockage for membrane with smaller pore size during filtration of small proteins, leading to the increase in irreversible fouling, which is in accordance with the high *Rir* value.

Overall, based on the fouling experiments, incorporating PAN-*g*-PVA copolymer additive to PAN-based membranes is proven to be useful for improving anti-fouling property of PAN membranes. However, it is difficult to provide a side-by-side comparison between the findings of this work with other published works due to the differences in the properties of copolymer additives used, the model foulants tested, the membrane configuration, etc. But, it is worth to mention that this is the first attempt concerning the modification of PAN membranes with this type of amphiphilic copolymer additive.

CONCLUSION

The correlation between composition of graft copolymer in dope solution and hollow fiber membrane properties and performance was investigated in terms of membrane morphological and surface properties, separation performance and fouling resistant. The variation in graft copolymer composition is found to induce formation of bigger finger-like voids near the inner and outer membrane as well as resulting in formation of macroporous substructure. The copolymer additive also plays a significant role in improving porosity and pore size of the membrane, in which highest pore size (45 nm) and porosity (27%) could be obtained from membrane prepared from highest graft copolymer content. On the other hand, the surface roughness of the membrane also increases with increasing copolymer content, mainly due to faster demixing process during phase inversion process. The incorporation of the PAN-*g*-PVA graft copolymer is also observed to influence membrane surface hydrophilicity in which contact angle decreases from 76° of PAN control membrane to 53° for the most hydrophilic membrane (CP10-5) due to variation in the degree of PVA surface coverage. The changes in membrane morphology, surface roughness and hydrophilicity are found to give significant contribution to the increase in pure water flux by which highest flux (~297 L/m^2·hr) is achieved by the membrane incorporated with highest copolymer content: CP10-20. With respect to anti-fouling property, it can be concluded the fouling resistance of the hollow fiber membranes during filtration of different types of proteins is mainly governed by the degree of PVA surface coverage and partly by surface roughness and pore size.

ACKNOWLEDGEMENT

The authors would like to acknowledge Ministry of Education (MOE), Malaysia for funding the research through Long-term Research Grant Scheme (LRGS, grant no. R.J130000.7837.4L803) for the research work conducted.

REFERENCES

1. P. Kanagaraj, S. Neelakandan and A. Nagendran, *Korean J. Chem. Eng.*, **31**(6), 1057 (2014).
2. Y. M. Lo, D. Cao, D. S. Argin-Soysal, J. Wang and T. S. Hahm, *Bioresour. Technol.*, **96**, 687 (2005).
3. Y. H. Teow, A. L. Ahmad, J. K. Lim and B. S. Ooi, *J. Appl. Polym. Sci.*, **128**, 3184 (2013).
4. A. Saxena, B. P. Tripathi, M. Kumar and V. K. Shahi, *Adv. Colloid Interface Sci.*, **145**, 1 (2009).
5. Y. Su, C. Li, W. Zhao, Q. Shi, H. Wang, Z. Jiang and S. Zhu, *J. Membr. Sci.*, **322**, 171 (2008).
6. N. A. M. Nazri, W. J. Lau, A. F. Ismail, T. Matsuura, D. Veerasamy and N. Hilal, *Desalination*, **358**, 49 (2015).
7. H. Yuan, J. Ren, L. Cheng and L. Shen, *J. Appl. Polym. Sci.*, **130**, 4066 (2013).
8. K. Y. Kim, E. Yang, M. Y. Lee, K. J. Chae, C. M. Kim and I. S. Kim, *Water Res.*, **54**, 62 (2014).
9. Z. Zhao, J. Zheng, M. Wang, H. Zhang and C. C. Han, *J. Membr. Sci.*, **394-395**, 209 (2012).
10. Z. Xu, X. Huang and L. Wan, *Surface Engineering of Polymer Membranes*, Springer, New York (2009).
11. D. S. Wavhal and E. R. Fisher, *Langmuir*, **19**, 79 (2003).
12. R. Q. Kou, Z. L. Xu, H. T. Deng, Z. M. Liu, P. Seta and Y. Xu, *Langmuir*, **19**, 6869 (2003).
13. P. Maheswari, P. Barghava and D. Mohan, *J. Polym. Res.*, **20**, 74 (2013).
14. M. Amirilargani, A. Sabetghadam and T. Mohammadi, *Polym. Adv. Technol.*, **23**, 398 (2012).
15. A. Asatekin, S. Kang, M. Elimelech and A. M. Mayes, *J. Membr. Sci.*, **298**, 136 (2007).
16. B. Liu, C. Chen, T. Li, J. Crittenden and Y. J. Chen, *J. Membr. Sci.*, **445**, 66 (2013).
17. Q. Shi, J. Q. Meng, R. S. Xu, X. Du and Y. F. Zhang, *J. Membr. Sci.*, **444**, 50 (2013).
18. H. Lohokare, Y. Bhole, S. Taralkar and U. Kharul, *Desalination*, **282**, 46 (2011).
19. B. Jung, J. K. Yoon, B. Kim and H. W. Rhee, *J. Membr. Sci.*, **246**, 67 (2005).
20. Q. Sun, Y. Su, X. Ma, Y. Wang and Z. Jiang, *J. Membr. Sci.*, **285**, 299 (2006).
21. X. Chen, Y. Su, F. Shen and Y. Wan, *J. Membr. Sci.*, **384**, 44 (2011).
22. N. A. M. Nazri, W. J. Lau, A. F. Ismail and D. Veerasamy, *Desalin. Water Treat.* (2014), DOI:10.1080/19443944.2014.932707.
23. N. A. M. Nazri, W. J. Lau, M. Padaki and A. F. Ismail, *J. Polym. Res.*, **21**, 1 (2014).
24. D. W. Kravelen, *Properties of Polymers: Their Correlation with Chemical Structure: Their Numerical Estimation and Prediction from Additive Group Contribution*, Elsevier, Amsterdam (2009).
25. Q. F. Alsalhy, *Desalination*, **294**, 44 (2012).
26. Y. H. Cho, H. W. Kim, S. Nam and H. B. Park, *J. Membr. Sci.*, **379**, 296 (2011).
27. N. Misdan, W. J. Lau, A. F. Ismail and T. Matsuura, *Desalination*, **329**, 9 (2013).
28. P. Harder, M. Grunze, R. Dahint, G. M. Whitesides and P. E. Laibinis, *J. Phys. Chem. B*, **102**, 426 (1998).
29. J. F. Hester, P. Banarjee and A. M. Mayes, *Macromolecules*, **32**, 1643 (1999).
30. D. Rana and T. Matsuura, *Chem. Rev.*, **110**, 2448 (2010).
31. R. Jamshidi Gohari, W. J. Lau, T. Matsuura and A. F. Ismail, *J. Membr. Sci.*, **446**, 326 (2013).